In vivo longitudinal photoacoustic imaging of subcutaneous tumours in mice

Jan Laufer[a], Peter Johnson[b], Edward Zhang[a], Bradley Treeby[a],
Ben Cox[a], Barbara Pedley[b], Paul Beard[a]
Department of Medical Physics & Bioengineering([a]) and the Cancer Institute([b]),
University College London, London WC1E 6BT, UK

ABSTRACT

Photoacoustic tomography can provide high resolution 3D images of vascular networks, making it well suited to characterising the development of tumour vasculature and its response to treatment. In this study, photoacoustic images to depths of up to 9 mm were obtained using an all optical ultrasound detection scheme. Two type of colorectal tumours (LS174T and SW1222) implanted subcutaneously in a mouse were studied. 3D photoacoustic images were obtained *in vivo* revealing the different vascular architectures of each tumour type and their evolution over a period of several days. The results suggest that photoacoustic imaging could play a role in providing essential pre-clinical information on tumour pathophysiology and eliciting the biological mechanisms underlying anti-angiogenic therapies and other treatments.

Keywords: Photoacoustic imaging, tomography, Fabry-Perot polymer film ultrasound sensor, tumour, angiogenesis

1. INTRODUCTION

The study of tumour angiogenesis is relevant to the pre-clinical development of new anti-cancer drugs. Current small animal imaging modalities include multiphoton microscopy [1], Doppler OCT [2], and x-ray computed tomography (CT) [3]. Optical methods such as multiphoton microscopy can provide high resolution images of tumour vasculature but usually requires the use of skin fold window chambers and is highly restrictive in terms of imaging depth (<1mm) and study duration. CT has been shown to provide excellent whole body images of the vasculature, including subcutaneous tumours. Its disadvantages are the requirement for contrast agents and the severe restrictions on the duration of longitudinal studies due to the typically high radiation doses.

Photoacoustic tomography is a new imaging modality based upon the generation of ultrasound by the absorption of short pulses of laser light in tissue. It provides both the high contrast of optical imaging methods and the high spatial resolution available to ultrasound. Since photoacoustic image contrast is largely absorption based it is particularly well suited to imaging the vasculature due to the strong optical absorption exhibited by haemoglobin. Furthermore it is non invasive and without harmful side effects. In this study, images of two types tumours implanted subcutaneously in mice were acquired noninvasively and imaged *in vivo* over a period of several days.

2. METHODS

2.1 Photoacoustic small animal imaging system

Figure 1 shows a schematic of the photoacoustic imaging system [4], the sensing mechanism of which is based on the interferometric detection of ultrasound. High energy excitation pulses were produced by a tuneable laser system (Quanta Ray Pro-270/premiScan, Newport Spectra Physics/GWU) and guided to the target using a multimode optical fibre. Following optical absorption in the tissue, the emitted photoacoustic waves are detected by a planar Fabry-Perot polymer film interferometer sensor. Its operation involves illuminating the interferometer using the output of a wavelength-tuneable cw interrogation laser and detecting the intensity of the reflected light. By tuning the wavelength to the steepest slope of the interferometer transfer function, acoustically induced modulations of the optical thickness of the interferometer are linearly detected as a change in the reflected intensity. By raster scanning the interrogation beam

Photons Plus Ultrasound: Imaging and Sensing 2011, edited by Alexander A. Oraevsky, Lihong V. Wang,
Proc. of SPIE Vol. 7899, DOI: 10.1117/12.876782

across the sensor, photoacoustic signals were acquired at multiple points from which 3D images were reconstructed using a time reversal technique [5-6]. A typical scan acquired 20000 waveforms, each of which contained 500 data points, and took 8min to complete.

The Fabry-Perot based imaging system has a number of advantages over conventional piezoelectric based photoacoustic detection schemes. The optical nature of the sensor allows it to be transparent to the excitation light enabling backward mode operation to be achieved, i.e. photoacoustic signal generation and detection occur on the same side of the target. It can provide very small element sizes (<50μm) with high acoustic sensitivity (0.3kPa over a 20MHz measurement bandwidth [4, 7]). In addition, the sensor has a highly uniform frequency response from DC to 30MHz (-3dB bandwidth). Importantly, this system operates in tomographic mode in which full field illumination is employed to excite the photoacoustic waves. As a consequence it can provide significantly greater penetration depths (~ 10mm) than optical resolution photoacoustic microscopy (OR-PAM) which is limited to depths of less than 1mm. The design of the scanner also enables it to be interfaced to the animal very straightforwardly. As shown in Figure 1, the sedated mouse simply rests on the Fabry-Perot sensor to which it is acoustically coupled with a small amount of water or ultrasound matching gel.

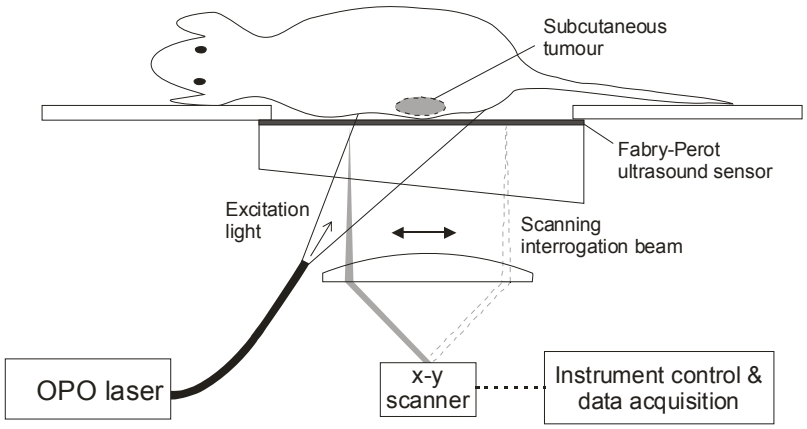

Figure 1 Schematic of the photoacoustic imaging system used to study subcutaneous tumours in nude mice.

2.2 Preparation of mouse models

Two human colorectal tumour cell lines (LS174, SW1222) with very different vascular architectures were studied. The tumours were grown subcutaneously in the flank of nude mice (MF1, nu/nu) by injecting a suspension of $5x10^6$ cells. Photoacoustic images were acquired between day 7 and 12 post-inoculation. The animals were anaesthetised using isofluorane and placed on the Fabry-Perot ultrasound sensor. An aqueous gel facilitated acoustic coupling. The beam diameter at the target was 2cm, which resulted in a fluence of <10mJ/cm^2 and thus significantly below the MPE for skin [8] at the wavelengths used in this study. Images were acquired at up to four excitation wavelengths between 600nm and 680nm over a detection aperture of up to 14mm x 14mm with a step increment of up to 100μm. Each image took about 8min to acquire.

3. RESULTS

Figure 2 shows maximum intensity projections (MIP) of a 3D photoacoustic image of a subcutaneous tumour (LS174T) acquired on day 5 post-inoculation. Subdermal blood vessels are located at depths of 0-1.5mm, while the tumour is located at a depth of 0.6mm-2.0 mm. Due to the short time between cell inoculation and experiment, the tumour is relatively small with a diameter of approximately 2.5mm and a depth of 1.4mm. Given that the injected cell suspension was colourless, the contrast produced by the tumour suggests a rapid development of its internal vasculature. Figure 2 also shows the blood vessel network surrounding the tumour, such as the subdermal vessels to a depth of about 1.5mm, and larger, deeper vessels at depths >1.5mm, which may be part of the muscle structure. The smallest blood vessels that could be resolved were approximately 70μm in diameter. This agrees well with the maximum lateral resolution, which is primarily determined by the step size, which was 70μm in this case.

Photons Plus Ultrasound: Imaging and Sensing 2011, edited by Alexander A. Oraevsky, Lihong V. Wang,
Proc. of SPIE Vol. 7899, DOI: 10.1117/12.876782

Figure 3 shows MIPs of images of a subcutaneous tumour (SW1222) acquired on day 7 and day 11 post-inoculation. The images provide evidence of the rapid growth in tumour size over this period. The image contrast produced by the tumour on day 11 is greater than that on day 5, which suggests a significant increase in tumour vascularity. The MIPs also allow an estimation of tumour size, which was found to increase from 4.6mm to 6.9mm in diameter within 4 days.

During angiogenesis, the production of growth factors by the tumour stimulates migration of neo-vasculature from surrounding normal vessels towards the tumour. This can result in a highly abnormal and tortuous vascular architecture compared to normal tissue vessels. We have previously found this to be particularly pronounced in SW1222 tumours by vascular corrosion casting [9-10]. Figure 4 which shows an expanded section of Figure 3b, confirms these results. Two tortuous feeding vessels that merge with an SW1222 tumour (day 11 post-inoculation) can be seen.

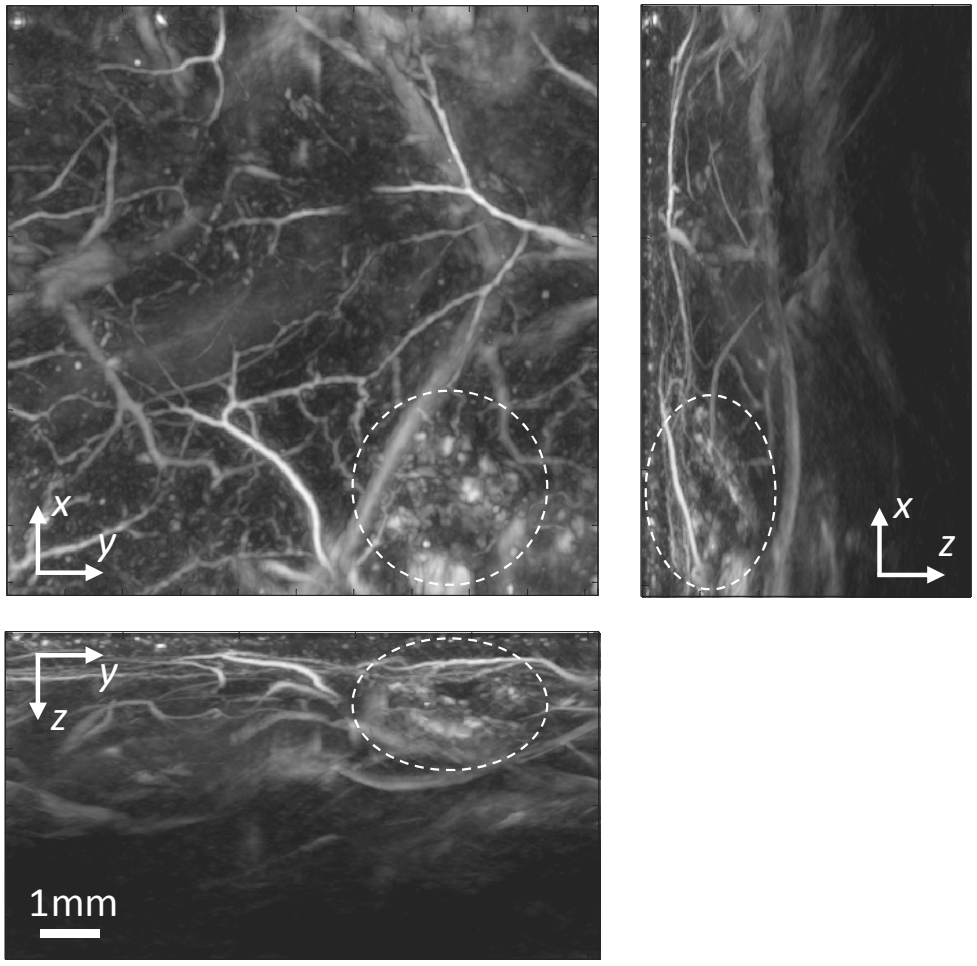

Figure 2 Maximum intensity projections of a 3D photoacoustic image showing an entire subcutaneous tumour (LS174T) on day 5 post-inoculation. The circles indicate the tumour location. The image was acquired at 658nm, its dimensions are 10mm x 10mm x 5.5mm, and the step size was 70μm.

Photons Plus Ultrasound: Imaging and Sensing 2011, edited by Alexander A. Oraevsky, Lihong V. Wang,
Proc. of SPIE Vol. 7899, DOI: 10.1117/12.876782

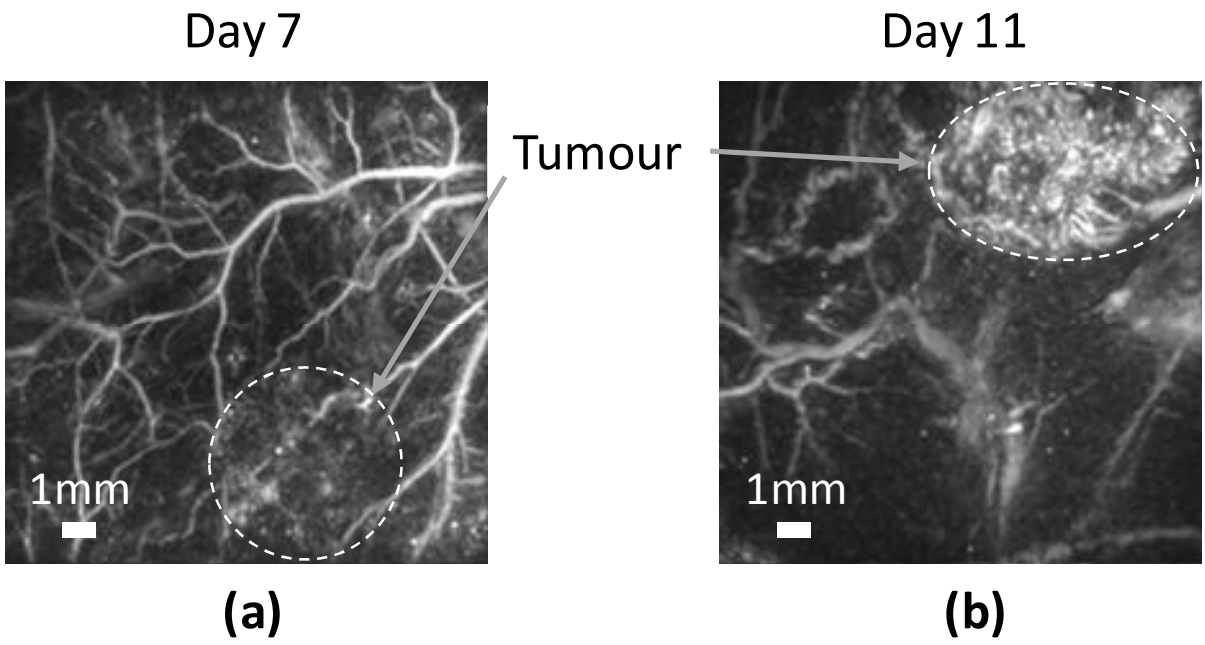

Figure 3 Maximum intensity projections (*x*-*y*) of 3D photoacoustic images acquired at 610nm showing the development of a tumour (SW1222) between day 7 (a) and day 11 (b). The images illustrate the growth of the tumour and the development of its vascularity as evidenced by a higher image contrast on day 11 compared to day 7.

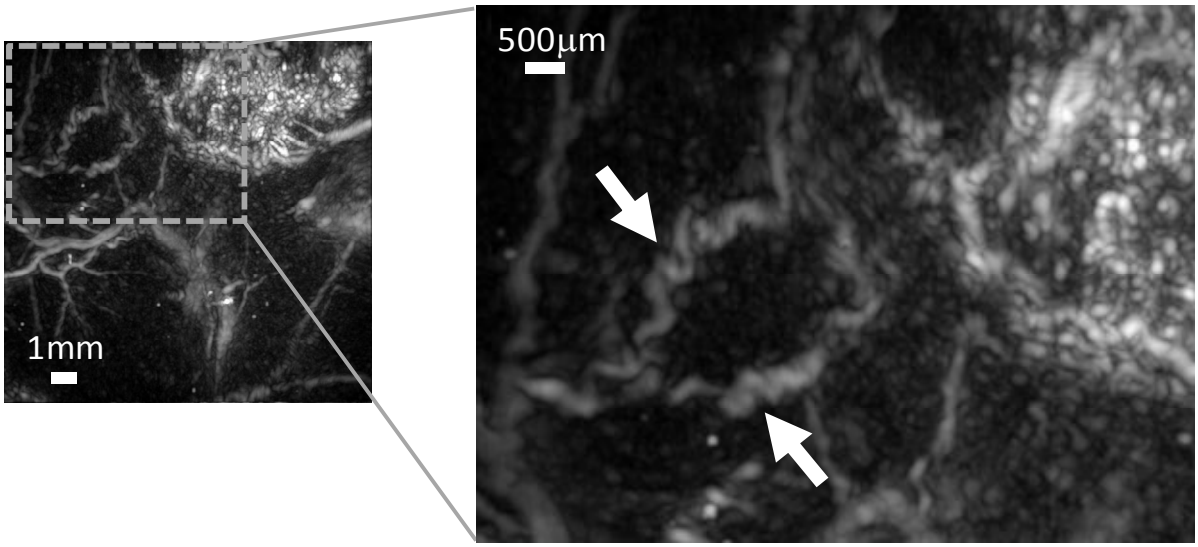

Figure 4 An expanded view of Figure 3(b), which shows an SW1222 tumour on day 11 post-inoculation. The arrows indicate two tumour feeding vessels, the shape of which has been become highly tortuous due to growth factors emitted by the cancer cells. The scan area was 14mm x 14mm with a step size of 100μm.

Photons Plus Ultrasound: Imaging and Sensing 2011, edited by Alexander A. Oraevsky, Lihong V. Wang,
Proc. of SPIE Vol. 7899, DOI: 10.1117/12.876782

Figure 5 shows photoacoustic images of two tumour models (LS174T, SW1222) together with representative examples of vascular corrosion casts obtained in tumours different to those imaged in this study. There is good qualitative agreement between the two modalities. The LS174T tumour, for example, is characterised by a heterogeneous distribution of blood vessel diameter and vessel density, and frequently contains avascular regions, which manifest themselves as voids in the resin casts. Some of these characteristics can be seen in the photoacoustic image, where absorbing regions of different sizes may be indicative of the heterogeneity in blood vessel diameter. By contrast, the corrosion cast of the SW1222 tumour shows a denser microvasculature and more homogeneous distribution in blood vessel diameter. This is confirmed by the photoacoustic image, which shows fine absorbing structures that are distributed relatively evenly across the tumour volume.

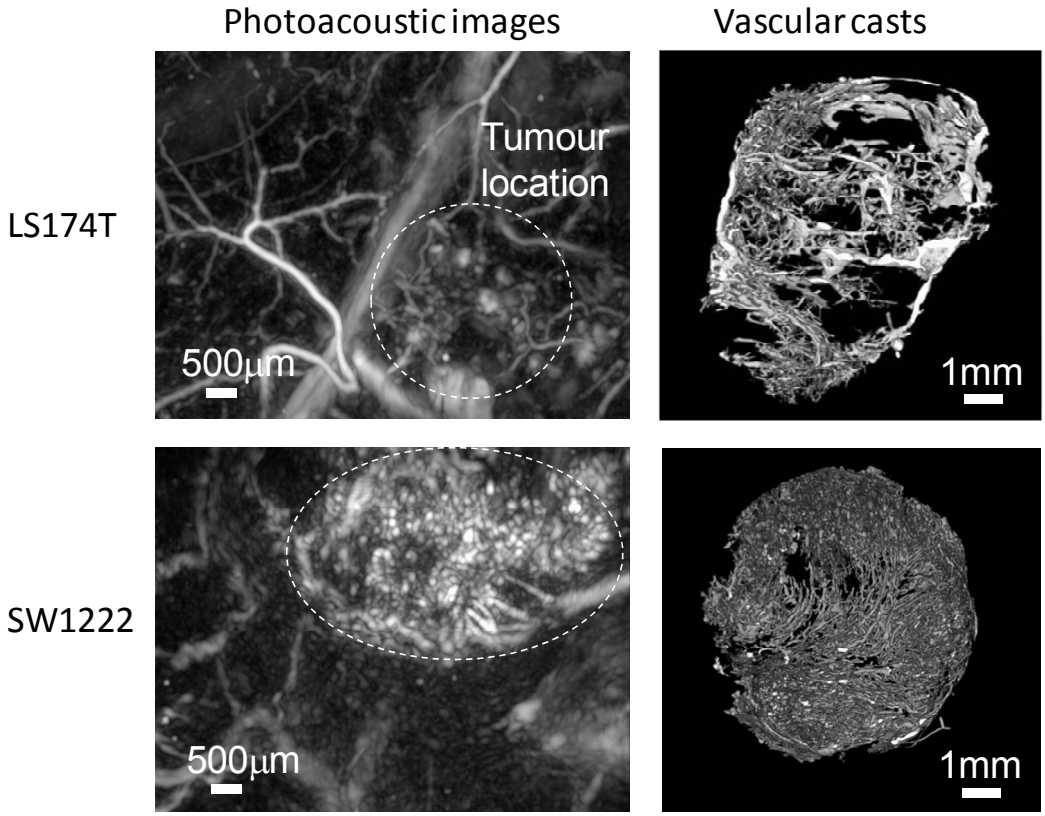

Figure 5 Qualitative comparison of photoacoustic images (MIP) of the two tumour models (LS174T, SW1222) with representative vascular corrosion casts (right hand column). The vascular structure of the tumours shown in the photoacoustic images agree well with those of the corrosion casts. The scan area of the photoacoustic images was 14mm x 14mm with a step size of 100μm.

4. CONCLUSIONS

High resolution 3D photoacoustic images of human tumours grown subcutaneously in mice were acquired in a non-invasive and longitudinal manner. A key component of this study was the photoacoustic imaging system based on a Fabry-Perot interferometer ultrasound sensor. This allowed high resolution 3D images over a lateral field of view of 15mm x 15mm to a depth of 9mm to be obtained thus enabling entire tumours to be visualised. The images showed the characteristic differences in the vascular architecture of the two different tumour models, rapid tumour growth and the vascular changes associated with tumour development. The results suggest that photoacoustic imaging may be able to contribute to the development of new cancer therapies. In particular, it could be used for longitudinal studies of the

efficacy of vascular disrupting agents, such as OXi4503, or the disruption and re-development of tumour vasculature following anti-angiogenic therapy.

REFERENCES

1. Tozer, G.M., et al., *Intravital imaging of tumour vascular networks using multi-photon fluorescence microscopy.* Advanced Drug Delivery Reviews, 2005. **57**(1): p. 135-152.
2. Vakoc, B.J., et al., *Three-dimensional microscopy of the tumor microenvironment in vivo using optical frequency domain imaging.* Nat Med, 2009. **15**(10): p. 1219-1223.
3. Kiessling, F., et al., *Volumetric computed tomography (VCT): a new technology for noninvasive, high-resolution monitoring of tumor angiogenesis.* Nat Med, 2004. **10**(10): p. 1133-1138.
4. Zhang, E., J. Laufer, and P. Beard, *Backward-mode multiwavelength photoacoustic scanner using a planar Fabry-Perot polymer film ultrasound sensor for high-resolution three-dimensional imaging of biological tissues.* Applied Optics, 2008. **47**(4): p. 561-577.
5. Treeby, B.E. and B.T. Cox, *k-Wave: MATLAB toolbox for the simulation and reconstruction of photoacoustic wave fields.* Journal of Biomedical Optics, 2010. **15**(2): p. 021314.
6. Treeby, B.E. and et al., *Photoacoustic tomography in absorbing acoustic media using time reversal.* Inverse Problems, 2010. **26**(11): p. 115003.
7. Zhang, E.Z., et al., *In vivo high-resolution 3D photoacoustic imaging of superficial vascular anatomy.* Physics in Medicine and Biology, 2009. **54**(4): p. 1035-46.
8. BSi, *British Standard*, in *BS EN60825-1*. 1994.
9. El Emir, E., et al., *Predicting Response to Radioimmunotherapy from the Tumor Microenvironment of Colorectal Carcinomas.* Cancer Research, 2007. **67**(24): p. 11896-11905.
10. Folarin, A.A., et al., *Three-dimensional analysis of tumour vascular corrosion casts using stereoimaging and micro-computed tomography.* Microvascular Research, 2010. **80**(1): p. 89-98.